THE JOURNAL OF PHYSICAL CHEMISTRY C

Article

pubs.acs.org/JPCC

Energy Transfer via Exciton Transport in Quantum Dot Based Self-Assembled Fractal Structures

César Bernardo,[†] I. Moura,*[,†] Y. Núnez Fernández,[‡] Eduardo J. Nunes-Pereira,[†] Paulo J. G. Coutinho,[†] Arlindo M. Fontes Garcia,[†] Peter Schellenberg,[†] Michael Belsley,[†] Manuel F. Costa,[†] Tobias Stauber,[§] and Mikhail I. Vasilevskiy[†]

[†]Centro de Física, Universidade do Minho, Campus de Gualtar, Braga, Portugal

[‡]Centro Atómico Bariloche, CONICET, 8400 Bariloche, Argentina

[§]Departamento de Física de la Materia Condensada, Universidad Autónoma de Madrid, Madrid, Spain

Supporting Information

ABSTRACT: Semiconductor quantum dot (QD) assemblies are promising systems for light harvesting and energy conversion and transfer, as they have a superior photostability compared to classical dyes and their absorption and emission properties can be tuned during synthesis. Here, we investigate excitonic energy transfer in self-assembled dentrite-type fractal structures consisting of QDs by microscopically mapping their fluorescence spectra and lifetimes. The behaviors of CdSe/ZnS and CdTe QD assemblies are compared; in particular, the energy transfer probability is found to be stronger in CdTe-based structures, scaling with their radiation quantum yield. Our results indicate Förster-type energy transfer in both systems, although with a higher efficiency in CdTe. The energy transfer is caused by near-field (nonradiative) dipole−dipole coupling between the individual QDs within a dendrite, with the excitation migrating from the edges to the center of the structure. The experimental findings are supported by theoretical modeling results obtained by using master equations for exciton migration/decay kinetics in diffusion-limited fractal aggregates composed of identical particles.

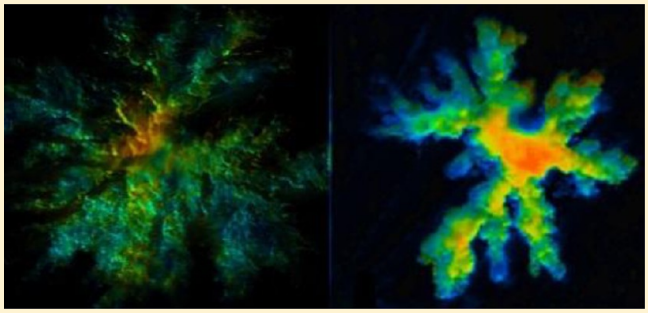

1. INTRODUCTION

Chemically synthesized quantum dots (QDs) of II−VI semiconductors are known for their excellent luminescent properties related to quantum-confined exciton states, which can be tuned by manipulating the particle size, shape, and composition and that show superior photostability compared to organic absorbers, allowing for many excitation−emission photocycles before irreversible bleaching. Among the numerous types of nanometer-scale building blocks, colloidal QDs are of special interest because they can form ordered assemblies, for example, for use in optoelectronic and biotechnology applications.[1] The main advantage of QDs-based structures over organic ones are their broad absorption band and the possibility of inter-nanodot energy transfer in nanocrystal-based solids.[2] Colloidal CdSe/ZnS and CdTe nanocrystal (NC) quantum dots are employed for the fabrication of self-assembled structures, which are aggregated assemblies that range in shape from nearly-1D nanowires to 2D and 3D structured systems.[3] The self-assembling process occurs at the liquid substrate interface,[4] where the competing effects of the fluid−solid phase transition, i.e., diffusion of NCs along the substrate surface and subsequent rupture of a thin liquid film on the substrate, lead to the formation of a large variety of different structures.[5] Nevertheless, the manipulation of QDs requires a detailed knowledge of the NCs chemistry and materials properties of the suspension fluids,[6] which is essential to control the NCs self-assembly mechanism.

In this context, a significant progress toward the development of patterned colloidal semiconductor NCs has been achieved during the past decade. The feasibility of self-organization of fluorescent CdTe NCs into crystalline nanowires in a water droplet has been demonstrated.[7] Their formation is supposed to be related to electrostatic attraction between NCs. Sukhanova et al. reported a novel route for the controlled, thermodynamically driven fabrication of even more complex hierarchical 2D arrays prepared from CdSe/ZnS water-solubilized NCs.[8] They found that water-solubilized QDs or quantum rods (QRs) formed homogeneously sized droplet-like spheroid clusters and hexagonal colloidal crystals by self-organization into more (QRs) or less (QDs) regular 2D assemblies.

An approach to obtain polycrystalline fluorescent dendrites from water-solubilized CdSe/ZnS QDs, making use of the self-assembly of NCs, has also been reported.[9] Their shapes can be

Received: November 21, 2013
Revised: January 21, 2014
Published: January 23, 2014

manipulated by controlling the water evaporation rate and the concentration of NCs (building blocks), allowing one to obtain dendrites with promising optical and energy transfer properties. Furthermore, it has been shown that a variety of nanostructures, such as nanowires or polycrystalline dendrites with desired properties (namely, size and morphology), can be achieved by controlling external parameters such as nanocrystal shape, concentration, and temperature.[10] Despite some progress in this field,[11−13] one of the major challenges is that the relationship between the NC interactions and the properties of the resulting self-assembled nanostructures remains to be fully elucidated. Specifically, the thermodynamic and kinetic factors, which govern the self-assembly process, are not well understood. Nevertheless, some of these structures are interesting for energy harvesting, where nonradiative transport of excitons competes with their recombination, providing a mechanism for energy transfer in a desired direction.

Fluorescence (Förster) resonance energy transfer (FRET) is an important energy transport mechanism at the nanoscale, first proposed for molecules more than 60 years ago.[14] As far as semiconductor quantum dots are concerned, this type of energy transfer was first demonstrated by Kagan et al. in specially designed films containing two different sizes of QDs acting as donors and acceptors, respectively.[15] They found that energy transfer of QDs in the solid state arises from dipolar coupling between proximal QDs and that the luminescence of the smaller dots is quenched by the large dots, whose emission in turn is enhanced. Since then, FRET processes in assemblies of closely spaced QDs have been demonstrated in a number of studies.[9,15−25] These works revealed that FRET between QDs, as well as in molecular systems, strongly depends on the interparticle distance, donor and acceptor concentration, the geometry of the system, and the dielectric environment. For example, Komarala et al. demonstrated FRET between CdTe QDs of different sizes, acting as donors and acceptors in the vicinity of gold nanoparticles.[16] They found that the FRET efficiency crucially depends on the distance between the monolayer of mixed donors and acceptors QDs and the Au nanoparticle layer. Although most of these studies used systems composed of different size QDs or mixtures of QDs with organic dye molecules, with predistributed roles of donors and acceptors,[17−19,26] it has also been shown that the energy transfer can proceed within a nominally monodisperse QD ensemble, directly from the "blue" to the "red" side of the luminescence band of several tens of meV in width.[20,21]The fluorescence lifetime is shorter at the "blue" side where QDs act mostly as donors. The time constant of the transfer was found to be on the order of 1 ns for CdSe QDs.[20] The decrease in the "blue" emission lifetime was larger for a higher (acceptor) QD concentration in the monolayer.[21] In a later work, the same authors studied FRET between donors and acceptors in a QD bilayer and found that energy migration within the donor layer (arising from intradonor ensemble FRET) has an impact on the donor−acceptor transfer.[22] Recently, it was demonstrated that the Förster radius, a signature of the energy transfer efficiency between QDs, can reach some 14−22 nm, i.e., values much higher than those usually quoted for molecular systems.[23] These results indicate that FRET processes can involve many exciton hops between QDs before they finally recombine, giving rise to nonradiative energy transport fluxes in QD assemblies. Although normally the exciton energy is conserved during the hops,[14] one can also expect down- or up-conversion processes accompanied by the absorption or emission of an optical phonon coupled to the QD exciton.[27] These processes become particularly intriguing if the emitting and absorbing entities are arranged into structures of a nontrivial geometry, such as fractals.[28] In particular, it has been suggested that a directed transfer from the periphery to the core can take place in QD dendrite structures.[9,25] This idea inspired the experimental and theoretical investigation reported in the present article.

CdSe/ZnS and CdTe QDs were synthesized in reverse micelles and aqueous solution, respectively, based on standard wet chemistry methods.[29,30] Thioglycolic acid was used to passivate the surface dangling bonds, thereby improving stability and surface functionality of the synthesized nanoparticles. As only the surface shell was altered by this procedure, the absorption and emission spectra remain largely unaffected.[1] These QDs were used to fabricate dendrite-type fractal structures, which are formed spontaneously during incubation and evaporation of the solvent. However, the morphology of these structures formed from either CdSe/ZnS or CdTe nanoparticles is distinctively different. The structures, of a certain fractal dimension, were studied using the microscopic fluorescence intensity and lifetime mapping. The energy transfer between QDs has been modeled using master equations for the exciton "occupation probabilities", with the transition rates decaying with the distance as $(R_F/r)^6$, where R_F is the Förster radius.[14,31] The modeling results show that the anisotropic energy transfer can indeed take place in fractal assemblies of monodisperse nanoparticles if the Förster radius is sufficiently large. It can lead to excitation energy funneling into the central part of the fractal structure. We do find indications of this effect in our experimental data (fluorescence lifetime maps), specifically for CdTe QD dendrites.

2. EXPERIMENTAL SECTION

2.1. Materials. Selenium powder (99.5%) was obtained from ACROS. Cadmium nitrate tetrahydrate (98%), sodium sulfide (98%), sodium bis(2-ethylhexyl)sulfosuccinate (AOT, 99%), hydrazine, 25% (w/w) sodium methoxide solution in methanol, zinc nitrate hexahydrate (98%), thiourea (99%), and thioglycolic acid (98%) were all acquired from Sigma-Aldrich. Aluminum telluride was purchased from Cerac Inc. All chemicals were used without further purification and treatment. Deionized water was used in all experiments. Aminoalkylsilane and polylysine microscope slides were purchased from Sigma-Aldrich.

2.2. Synthesis of CdSe, CdSe/ZnS, and CdTe. The synthesis of CdSe remained essentially the same as reported previously.[29] The concentration of AOT in cyclohexane was adjusted to 0.15 M as well the solvent (DMSO) to prepare the polyselenide solution used as precursor.

CdSe/ZnS nanoparticles were prepared as follows: 13 μL of aqueous solution of zinc nitrate hexahydrate (0.2 M) and the same volume of aqueous thiourea solution (0.2 M) were added to 2 mL of AOT in cyclohexane in different flasks; both solutions were subjected to vortexing. Afterward, the resulting microemulsion containing zinc nitrate hexahydrate was added, drop by drop, to an already-prepared solution of CdSe in AOT/cyclohexane (2 mL), synthesized under the conditions described above, followed by the addition of 2 mL of the microemulsion containing thiourea, under strong stirring. The solution was sealed and heated during 2 h at 70 °C. After completing the CdSe/ZnS synthesis process, nanocrystals were washed twice with methanol and cyclohexane. Subsequently,

dx.doi.org/10.1021/jp411456m | J. Phys. Chem. C 2014, 118, 4982−4990

the AOT was exchanged by a thiol containing compound (TGA). QDs were precipitated out by centrifugation at 9000 rpm, washed with methanol, and subsequently dried under nitrogen. CdTe QDs stabilized with TGA were synthesized in an aqueous solution according to the procedure described by Byrne et al.[30]

2.3. Spectroscopic Measurements. Absorption spectra of the QDs solutions were recorded using a Shimadzu UV-3101PC UV−vis−NIR spectrophotometer. The photoluminescence (PL) spectra were taken with a Fluorolog 3 fluorescence spectrometer with an excitation wavelength of 360 nm provided by a xenon lamp. All the optical measurements were performed under ambient conditions. The PL spectra were corrected, and the quantum yields (QYs) were determined using Rhodamine B in ethanol (QY = 70%) as a reference.[32]

The time-resolved fluorescence decay measurements were done using time-correlated single photon counting (TCSPC). In this setup, the samples were excited using the direct output at 800 nm of a femtosecond Coherent Mira titanium−sapphire laser (two-photon absorption) or its frequency-doubled output at 400 nm (one-photon absorption) and the fluorescence collected at 90° from the incident beam.

The detection wavelength range was selected by a small double monochromator (Spectral Products CM110 1/8m Czerny-Turner). A polarizer set to the magic angle compensated for rotational depolarization, and a $\lambda/2$ achromatic wave plate was used to rotate the polarization to maximize the signal transmitted by the monochromator. A multichannel plate (MCP) photon counting photomultiplier (Hamamatsu R3809U-51) served as the photon detector. Subsequently, the data were collected using a Becker & Hickl SPC-150 photon counting computer board. The overall time resolution of the setup was 20 ps.

2.4. Preparation of Self-Assembled Fractal Structures. The experiments were carried out in aliquots of water solutions of water-solubilized CdSe/ZnS and CdTe capped dots with TGA, using different concentrations. Sodium hydroxide was added to the water solutions in order to control the fraction of ionization of the QDs. Aliquots of prepared solutions are applied to microscope slides coated with aminoalkylsilane and polylysine and with the glass having been previously cleaned by plasma etching with argon. The experiments were performed under an ambient atmosphere at room temperature.

2.5. Fluorescence Intensity and Fluorescence Lifetime Microscopy. The characterization of self-assembled structures immobilized on substrates was performed employing fluorescence intensity and fluorescence lifetime microscopy. Fluorescence images were taken with a Leica DM4000 B microscope with a digital color camera Leica DFC310 FX. Fluorescence lifetime mapping was performed using a home-made Fluorescence lifetime imaging microscope (FLIM) based on the instrumentation described in 3.2. To prevent distortion a *xy*-stage moved the microscopy slide through the excitation beam, and the light was collected using a 100× Mitutoyo Plan Infinity-Corrected Long WD Objective. The overall time resolution of the FLIM setup was 20 ps, and the spacial resolution was around 0.7 μm. The fluorescence spectra of individual locations were taken in the same setup by coupling the emitted light through a glass fiber into a spectrometer (Shamrock SR-303i) equipped with a CCD camera (Andor Newton 920).

3. DATA PROCESSING AND MODELING

3.1. Dendrite Morphology. The box-counting algorithm[33] was used to calculate the fractal dimension of the planar images of the self-assembled QD dendrites. After performing digitalization of the microscopic images, a grid of box length ε was applied to the obtained gray scale maps, and the number of boxes, $N(\varepsilon)$, required to cover the entire dendrite was counted. According to Mandelbrot,[33] this number scales with ε as

$$N(\varepsilon) \propto \varepsilon^{D} \tag{1}$$

where D is the fractal (Hausdorff) dimension of the structure. It follows from eq 1 that D can be determined from a double-logarithmic plot of $N(\varepsilon)$ as

$$D = \lim_{\varepsilon \to 0}[-\log N(\varepsilon)/\log \varepsilon] \tag{2}$$

We also determined the autocorrelation function of the microscopic images, defined by eq S1 in the Supporting Information, and analyzed its spatial variation.

3.2. Lifetime Determination from Luminescence Decay Kinetics. The measured fluorescence decay kinetics are essentially nonexponential, as typical of ensembles of emitters even if each of them can be characterized by a single radiative lifetime. Several approaches are possible to analyze such complex decays.[34−36] The simplest one is to use a sum of exponentials, even though no clear physical meaning usually can be ascribed to each component. For an ensemble of emitting particles, one can expect a continuous distribution of lifetimes and analyze the characteristics of this distribution, $f(\tau)$ (probability density function, PDF).[34−36]

$$I(t) = I(0)\int_0^\infty f(\tau)\exp\left(-\frac{t}{\tau}\right)\mathrm{d}\tau \tag{3}$$

According to the definition (3), the PDF can be obtained from the normalized decay kinetics, $I(t)/I(0)$, through the inverse Laplace transformation. It has been shown by Berberan-Santos et al.[35,36] that the statistical moments of the PDF (denoted by $\langle\tau^n\rangle$) can be related to those of the decay kinetics itself, defined by

$$\overline{\tau}^n = \frac{\int_0^\infty I(t)t^n\,\mathrm{d}t}{\int_0^\infty I(t)\,\mathrm{d}t}; \qquad n = 1, 2, \ldots \tag{4}$$

The first moment, $\overline{\tau}$, is the familiar mean (radiative) lifetime, and it is given by $\overline{\tau} = \langle\tau^2\rangle/\langle\tau\rangle$. This lifetime will be presented in the form of maps obtained from the decay kinetics measured at different locations within the same structure, thus allowing for direct comparison of experimental and calculated results.

3.3. Master Equations for Modeling Exciton Transport. Let us assume that a fluorescent particle (an isolated QD), when excited, emits a single photon with a rate constant γ, which corresponds to the radiative recombination of the confined exciton in its ground state (and the inverse of γ is the unquenched fluorescence lifetime[37]). We want to calculate the instantaneous polarization of an ensemble of such particles after an excitation pulse. The particle is polarized when it contains an exciton. If the particles do not interact, the related "occupation probability" of any of them, n_i, is simply given by $\mathrm{d}n_i/\mathrm{d}t = -\gamma n_i$. By this, we assume that the presence of the other fluorescent particles does not affect the radiative lifetime of an isolated QD, which becomes exact in the limit of point-like quantum emitters. However, in the presence of other quantum absorbers

dx.doi.org/10.1021/jp411456m | J. Phys. Chem. C 2014, 118, 4982−4990

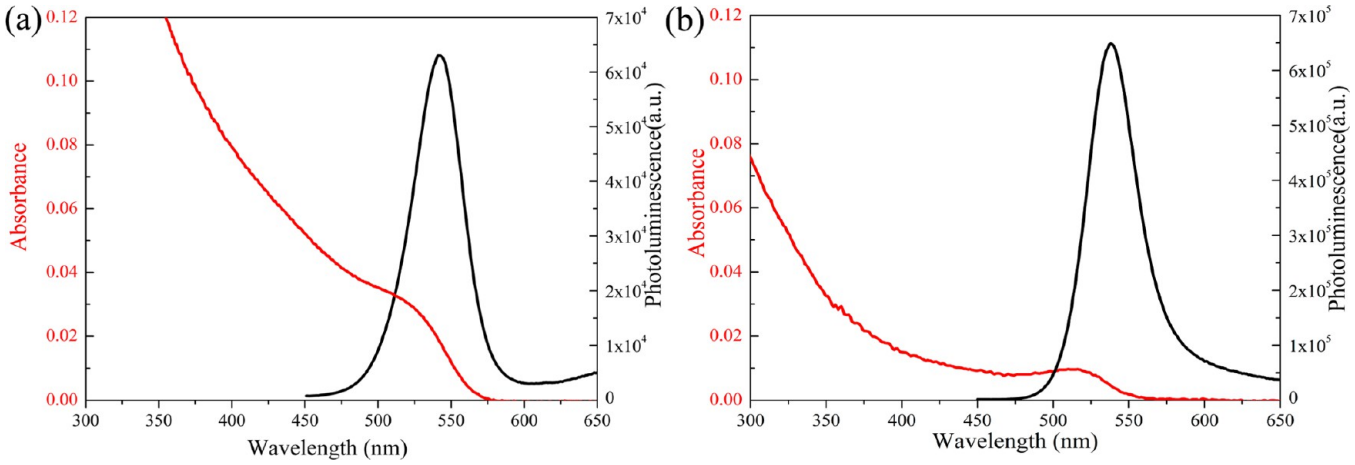

Figure 1. PL and UV−vis absorption spectra of as-prepared (a) CdSe/ZnS and (b) CdTe quantum dots capped with thioglycolic acid dissolved in water.

in the neighborhood, there is an additional decay channel due to near-field dipolar interaction, which leads to a depopulation and a repopulation term in the rate equation.[14] This decay channel shall be characterized by the probability per unit time, $W_{i\to j}(r)$, and the kinetic equation becomes as follows:

$$\mathrm{d}n_i/\mathrm{d}t + \gamma n_i = -\sum_{j\neq i} W_{i\to j} n_i(1-n_j) + \sum_{j\neq i} W_{j\to i} n_j(1-n_i) \tag{5}$$

Two terms on the right-hand side of eq 5 describe the forward and backward transfer processes. If the energy is conserved in the transfer process, we have $W_{i\to j} = W_{j\to i}$ and the nonlinear terms cancel. We thus end up with a system of linear differential equations for the occupation numbers, which can be written in a compact form:

$$\mathrm{d}\mathbf{P}/\mathrm{d}t = \mathbf{\Gamma}\cdot\mathbf{P} \tag{6}$$

where $\mathbf{P}(t)$ is an N-component vector of the occupation numbers and the matrix $\mathbf{\Gamma}$ is defined by

$$\mathbf{\Gamma} = -(\gamma + \sum_{k\neq i} W_{i\to k})\delta_{ij} + W_{j\to i}(1-\delta_{ij}) \tag{7}$$

where δ_{ij} is Kronecker's symbol. Even though eq 5 may look quite simple, its solution for an arbitrary distribution of particles in space is cumbersome.[31] The usual simplification is to neglect the backward transfer (the second term in eq 7). Then, assuming further that the acceptors are uniformly distributed in space, an analytical solution of (6) is possible,[38] leading to the so-called stretched exponential decay of the average population of excited particles, $P(t) \equiv \langle \mathbf{P}(t) \rangle$ (where the angular brackets mean average over the distribution of acceptors)

$$P(t) \propto \exp[-\gamma t - C(\gamma t)^{D/6}] \tag{8}$$

where C is a constant and D is the dimension of the system. Although eq 7 was originally derived for a dilute two-dimensional system,[38] it has been extended to fractals, in the so-called Förster limit (low donor/high acceptor concentration).[39,40] According to Pines et al.,[39] back-transfer between donors diminishes the prefactor C by a factor of $2^{(1-D/6)}$. Relation 8 gives insight into the understanding the fluorescence decay kinetics affected by the energy transfer processes, at least, at short times after the excitation pulse, before exciton migration between donors becomes important.

However, in order to describe our experiments, we shall require the population of excited particles averaged locally, within the fluorescence collection window. Therefore, we cannot directly use eq 8 and shall not neglect backward transfer. We shall assume that the particles forming our QD dendrite are some identical light absorbing and emitting entities (i.e., donors and acceptors at the same time), which are coupled by *reversible* Förster-type energy transfer processes, with the probability per unit time given by Förster[14]

$$W_{i\to j}(r) = \gamma(R_\mathrm{F}/r)^6 \tag{9}$$

where the indices i and j refer to any two of the particles, R_F is the Förster radius, and r is the interparticle distance. The exponent in eq 9 corresponds to the dipole−dipole interaction between the particles. The Förster radius is just the distance between the donor and acceptor at which the QD exciton recombination and nonradiative transfer probabilities are equal. It can be calculated quantum mechanically,[41,42] but here we will treat it as a phenomenological parameter. Qualitatively, it is determined by the overlap of the emission and absorption spectra of the donor and acceptor, respectively. Note that it is convenient to measure time in units of γ^{-1}; then R_F is the only parameter in eqs 8 and 9.

In order to solve eq 6, we express $\mathbf{P}(t)$ in terms of the eigenvalues and eigenvectors of the matrix $\mathbf{\Gamma}$ (denoted by $\{\lambda_i\}$ and $\{\mathbf{p}_i\}$, respectively):

$$\mathbf{P}(t) = \sum_{i=1,N} A_i \mathbf{p}_i \exp(\lambda_i t) \tag{10}$$

The coefficients A_i can be obtained from the initial conditions, $\mathbf{P}(t{=}0) = \mathbf{P}_0$ (where $\mathbf{P}_0$ represents the particles excited by the laser pulse), by inverting the matrix $\mathbf{\Gamma}$, i.e., $\mathbf{A} = \mathbf{\Gamma}^{-1}\cdot\mathbf{P}_0$.

For numerical experiments, we generated fractal aggregates of particles that mimic the experimentally studied dendrites with the dimensionality $D \approx 1.7-1.8$, which is close to the value known for clusters obtained by so-called diffusion-limited aggregation (DLA).[43] Then, for a given DLA fractal distribution of QDs, the master equations were solved as described above, yielding the population of excited particles $\mathbf{P}(t)$, which was summed over the particles within the fluorescence collection window considered as a circle of a certain radius, $P(t) = \sum' n_i(t)$. By moving the center of the collection circle over the structure, we obtained maps of fluorescence decay kinetics that

dx.doi.org/10.1021/jp411456m | J. Phys. Chem. C 2014, 118, 4982−4990

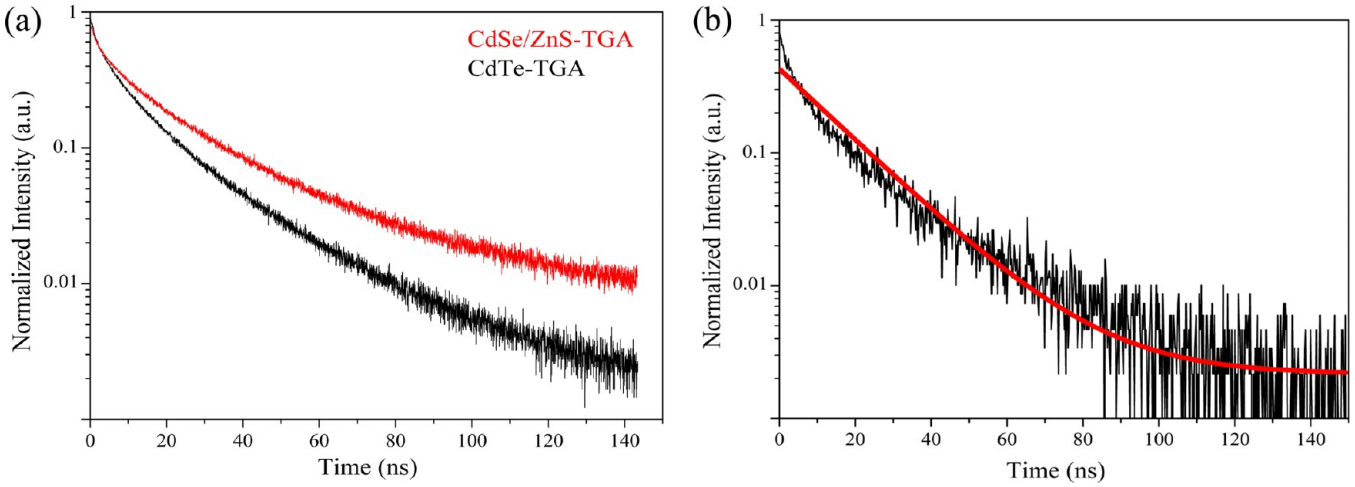

Figure 2. Decay curves of (a) CdSe/ZnS and (b) CdTe quantum dots, with a (multiexponential) fit shown in (b), used to calculate the statistical moments as defined by eq 4.

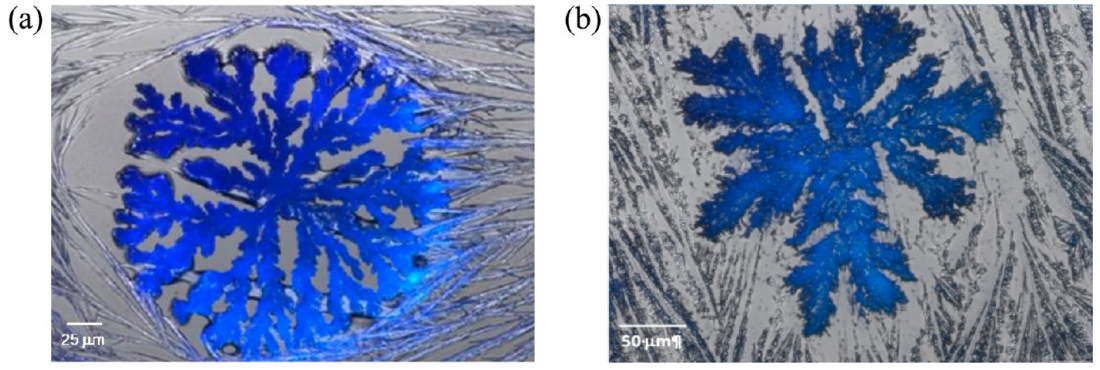

Figure 3. Examples of dendrite-type fractal structure made of (a) CdSe/ZnS and (b) CdTe capped with thioglycolic acid self-assembled on glass coated with polylysine.

were analyzed in the same way as experimental ones, as explained in section 3.2.

4. RESULTS AND DISCUSSION

4.1. Absorption and Emission of QDs in Solution. Figures 1a and 1b show the absorption and photoluminescence spectra of as-prepared CdSe/ZnS core/shell nanoparticles and CdTe QDs, respectively. From Figure 1a, a strong band in the UV range with a long tail ranging into the visible with several maxima can be seen. The most red-shifted is centered around 520 nm and is related to the size of the quantum dot. The width is due to the size distribution and differences in morphologies of the QDs. The resulting CdSe/ZnS PL emission peak has a full width at half-maximum (fwhm) of 39 nm and is centered around 541 nm. CdSe QDs were capped with ZnS, which decreases their vulnerability to impurities and lattice defects. The addition of ZnS shell also improved the fluorescence quantum yield due to the better passivation of the surface. The inorganic shell was grown over the core (CdSe), covering up dangling bonds on the core surface. After synthesis, CdSe/ZnS was precipitated followed by solubilization in water and QY of 1% was achieved.

For CdTe dots (Figure 1b) the absorption band related to the lowest confined exciton state is centered at 515 nm, the emission peak is centered at 538 nm, and the QY calculated from CdTe QDs water solution is 13%. The PL band fwhm is about 38 nm, which indicates that the particles are slightly more uniform in size compared to CdSe/ZnS. Using an empirical relationship between the absorption wavelength of the first excitonic absorption peak and the quantum dot size,[44] a diameter of 2.39 nm for the CdSe core and 2.71 nm for the CdTe particles size were estimated. The value for the CdSe core is probably an overestimate as the absorption and emission peaks of CdSe/ZnS can be slightly red-shifted from the corresponding plain CdSe QDs.[45] Assuming a 3 ML (molecular layer) ZnS shell, an additional 1 nm is expected for the particle diameter.[45] Thus, the size of the CdSe/ZnS core/shell QDs is expected to be slightly bigger than that of CdTe.

Figure 2a shows the fluorescence decay in water for CdSe/ZnS and CdTe NCs, both capped with TGA, and Figure 2b presents the decay kinetics with a multiexponential fit.[36]

We notice that in both materials the decay is not monoexponential already in the dilute solution environment. Moreover, the fluorescence decay rate for CdSe/ZnS NCs strongly depends on the probing (i.e., emission) wavelength as illustrated in Figure S2a of the Supporting Information. This implies that even for isolated QDs the PL kinetics are characterized by a distribution of decay rates, which may represent several different physical mechanisms including relaxation of carriers, influence of surface states, etc.[34] However, as this distribution is not very broad, we do not expect that it will impede the observation of the kinetic effects introduced by the FRET processes when these dots are arranged into self-assembled compact structures.

dx.doi.org/10.1021/jp411456m | J. Phys. Chem. C 2014, 118, 4982−4990

4.2. Self-Assembled Fractal Structures. CdSe/ZnS and CdTe dots capped with TGA were prepared according to the procedure described above and applied to microscope slides coated with different substrates. Saturation was achieved by gradually evaporating solvents in an ambient atmosphere. Under these experimental conditions, the solvent evaporation should be slower than the structure formation. They should remain relatively stable, since their growth rate might be higher than that of solvent evaporation. In other experiments performed at 50 °C the solvent evaporation rate was significantly increased which precluded the formation of structures, since generally slow growth is crucial to obtain highly ordered structures.

These results show that CdSe/ZnS and CdTe capped dots, at relatively low concentrations, formed dendrite-type structures that were considerably different in terms of morphology (see Figure 3). Highly organized and symmetric dendrites were observed using CdSe/ZnS, in contrast to those obtained with CdTe dots. Moreover, polylysine seems to be the best hydrophilic substrate to fabricate self-ordering dendrite-type structures, with droplets of colloidal suspension drying on their polar surface.

The fractal dimension (D) of prepared self-assembled structures was determined as described in section 3.1. The values obtained for CdSe/ZnS and CdTe were 1.74 and 1.68, respectively. The characteristic size of the CdSe/ZnS structure (shown in Figure 3a) is 32.0 ±1.2 μm, and that of the CdTe dendrite (Figure 3b) is 49.6 ± 1.6 μm. Although the values of D are similar for both fractals, the shape looks rather different. The difference can be related to the different physicochemical properties of two types of nanocrystals used for the preparation of self-assembled structures and to the solvent evaporation rate, which is different for the two preparation routes, owing to the different surface tension induced by both QDs solutions spread on the substrate surface.

4.3. Fluorescence Intensity and Fluorescence Lifetime Microscopy of Self-Assembled Fractal Structures. The optical properties of self-assembled fractal structures formed from CdSe/ZnS and CdTe QDs have been investigated by fluorescence intensity and fluorescence lifetime imaging microscopy.

Figure 4 illustrates the spatial distributions of the fluorescence lifetime for CdSe/ZnS and CdTe QD structures. It was observed that the former exhibits an almost homogeneous decay time throughout the structure, with a slightly longer lifetime in the outer parts of the dendritic structure. Contrary to this, the structure formed by CdTe shows a considerable variation across the structure, with a faster decay in the edges compared to the center of the superstructure (see Figure 5). This observation is in agreement with the results of our numerical simulations assuming energy transfer by dipolar near-field coupling between the individual QDs within a dendrite, presented in the next section. It can be shown that the decay time distributions depend on the Förster radius, and the exciton transfer effect is stronger in CdTe compared to CdSe/ZnS structures. The higher quantum yield of CdTe QDs (compared to CdSe/ZnS nanoparticles) increases the interdot coupling strength and, consequently, the Förster radius ($R_F \propto QY^{1/6}$).[14,46]

While Figures 4c,d show as an example the decay time distribution patterns recorded at 540 nm, the data for other probing wavelengths for the same structure are qualitatively similar. However, analogous to the dependence of fluorescence lifetime on the probing wavelength in solution (see Figure 2a), there is a similar dependence observed in the superstructures with a shorter lifetime corresponding to a shorter emission wavelength and a longer lifetime corresponding to a longer wavelength. Furthermore, the spread of decay times in absolute value as well as in percentage was smaller in the blue-shifted emission case which is correlated to the faster decay.

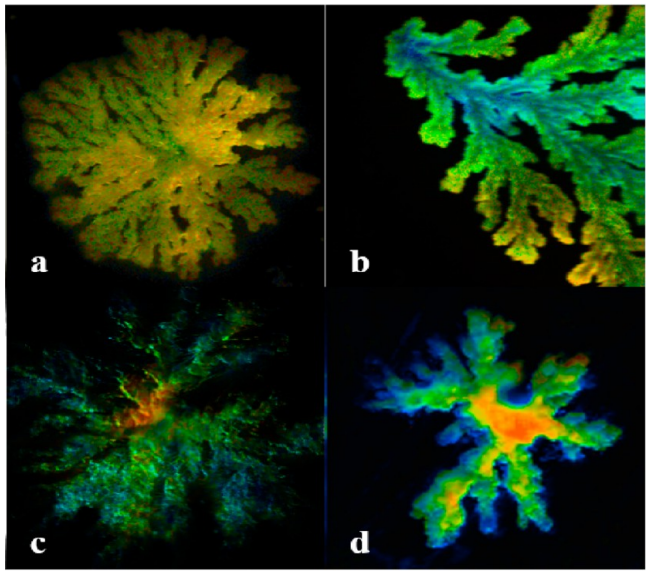

Figure 4. FLIM images of four representative superstructures obtained from CdSe/ZnS (a, b) and CdTe (c, d) QDs capped with thioglycolic acid, deposited on glass coated with polylysine. The emission wavelength is 545 nm for CdSe/ZnS and 540 nm in the CdTe structure. For CdTe dots, the spread of lifetimes is between 10 and 16 ns in the images. Each image has an independent color scale ranging from low (blue) to high lifetime values (red).

To exclude a possible inhomogeneity of the average nanocrystal size between the center and the outskirts of the structure as a possible reason for the observed decay time variation, selected spots in the superstructure were probed with fluorescence spectroscopy. As the emission wavelength strongly depends on the particle size, this should give the indication of an inhomogeneous average particle size distribution within the nanostructure. Figure 5 shows the location of individual probing spots in different structural elements of the structure. The spectral shift from the edges to the center is below 1 nm, and the spectra have all the same width. Thus, there is no variation of QDs size within the superstructure. We also checked another issue related to the spatial distribution of the decay rate PDF. The normalized amplitude of the dominant decay component obtained by the fitting (i.e., the PDF maximum value) was found quite uniform throughout the whole structure, for both CdSe/ZnS and CdTe dots (see Supporting Information). It means that the radiative properties of the dots themselves do no not vary along the structure Thus, all our experiments indicate nonradiative energy transfer as a result of exciton migration between individual quantum dots, mediated by their electromagnetic coupling. The effect was found stronger for CdTe compared to CdSe/ZnS structures, scaling with their radiative QY. All the experimental findings are supported by the results of modeling using master equations for exciton occupation and migration probabilities.

4.4. Energy Transfer Modeling Results. Using the formalism described in section 3.3, we performed the modeling

dx.doi.org/10.1021/jp411456m | J. Phys. Chem. C 2014, 118, 4982−4990

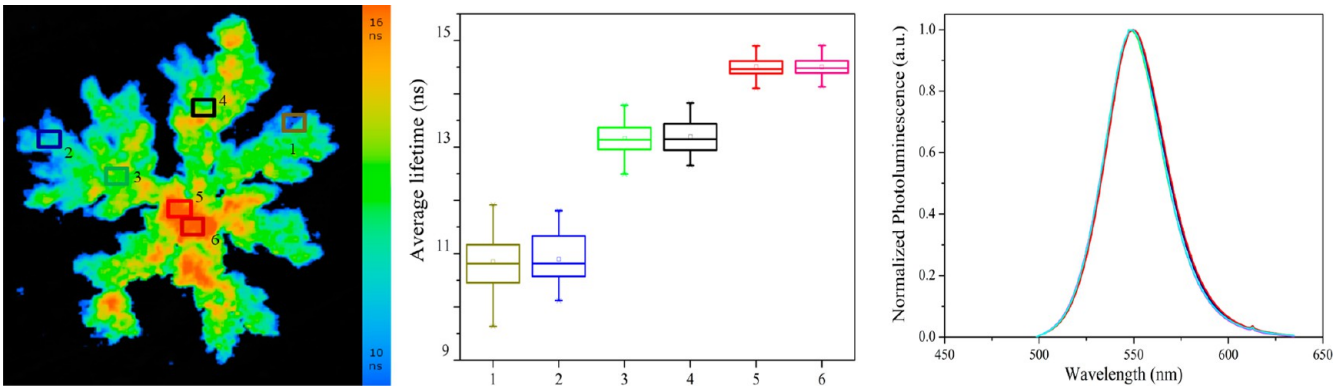

Figure 5. Average lifetime (first moment of decay kinetics) for a CdTe QD fractal superstructure. The lifetime is color coded according to the scale in nanoseconds (left); variation of the average lifetime between the selected zones (middle); fluorescence spectra of the selected zones (right).

of the energy transfer in a computer-generated planar fractal structure that has been excited locally, within a spot of size R_C (measured in units of QD radius for convenience as well as the Förster radius). The same spot was considered as the fluorescence collection window. The kinetics shown in Figure 6 correspond to the emission within the collection window, proportional to the excitation at a time t, i.e., $P(t) = \sum' n_i(t)$.

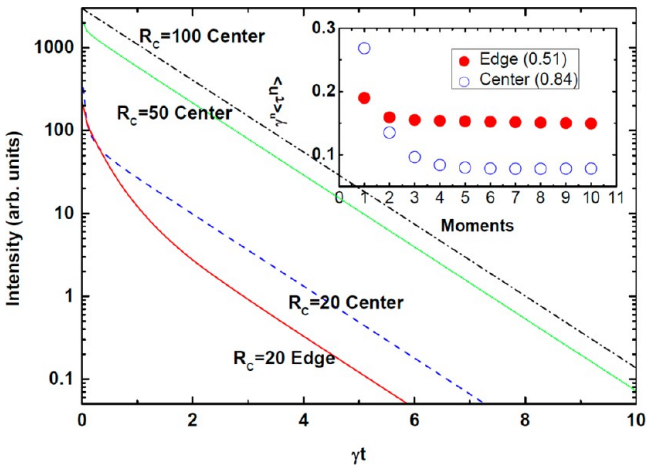

Figure 6. Calculated kinetics of the excited state population averaged over different collection areas (its radius in units of R is indicated on the plot), for $R_F/R = 5$. The inset shows the moments of the lifetime distribution PDF calculated for two decay kinetics corresponding to $R_C/R = 20$. The legend includes the radiative lifetimes, the ratio of the first two moments of the lifetime distribution. The radiative lifetimes are also shown in Figure 7.

First, let us note that the size of the collection window is important for the decay kinetics. When it is so large that the window includes the whole structure, the decay is simply exponential because all the transfer processes compensate each other (the case of $R_C/R = 100$). As the collection window includes only part of the structure, deviations from the simple exponential kinetics appear, since the Förster radius is sufficiently large to make transfer processes important. For $R_C/R = 20$ we observe a clear difference between the kinetics "measured" with the collection window located at the center or in the outskirts of the structure (Figure 6). This difference is clearly seen from the histograms of the PDF moments. The decay for $R_C/R = 20$ (center) corresponds to a broader PDF than for the edge.[a] It means that the former is more affected by the transfer processes because the QD density is higher in the core region. At the same time, the mean lifetime ($\bar{\tau}$) given by the ratio of the first two PDF moments is *longer* in the center of the fractal structure, in agreement with our experimental findings. The reason is the reversibility of the interdot transfer processes.

Simulated mean lifetime maps are presented in Figure 7. There is a clear difference between the cases of small ($R_F/R = 1$) and large ($R_F/R = 5$) Förster radius (note that for $R_F/R = 0$ the spatial distribution of the lifetime is completely uniform). As can be seen from Figure 7, in the case of $R_F/R = 5$ the lifetime is longer in the center of the structure. QDs located there have a smaller number of possible addresses for energy transfer than those in the periphery. For small Förster radius ($R_F/R = 1$) we can notice that a similar effect takes place at a smaller spatial scale, there are spots of longer lifetime located in some branches in the periphery. This can be understood by remembering that fractals are self-similar objects; i.e., the same properties can be revealed at different length scales. We would like to point out that the difference in the lifetime between the center and outskirts of the dendrite structure, seen in the calculated map for $R_F/R = 5$ (Figure 7a) and observed in our experiments, is not just a density effect. Fluorescence intensity maps (presented in Supporting Information) look very similar for *any* value of the Förster radius, with stronger emission in the center, which is accounted by the higher QD density in the dendrite core.

5. CONCLUSION

We have shown that CdSe/ZnS and CdTe nanoparticles synthesized by standard wet chemistry methods can be assembled into fluorescent dendrites and have investigated their time-resolved emission and exciton energy transfer properties. We found that the physicochemical properties of the nanoparticles as well as the substrate influence the shape of the self-assembled superstructures, even though their fractal dimensions can be similar. Along with the quantum yield of the dots, these factors have a significant impact on the energy transfer properties of the superstructures. While the importance of high quantum yield for energy transfer is obvious, the role of other factors is less clear, and it requires further investigation to understand why energy transfer is observed only in some cases. For instance, in a recent work[26] it could be only observed when dendrites were formed from nanoparticles integrated with J-aggregates but not for structures formed just from QDs of similar sizes. Nevertheless, we have been able to demonstrate

dx.doi.org/10.1021/jp411456m | J. Phys. Chem. C 2014, 118, 4982−4990

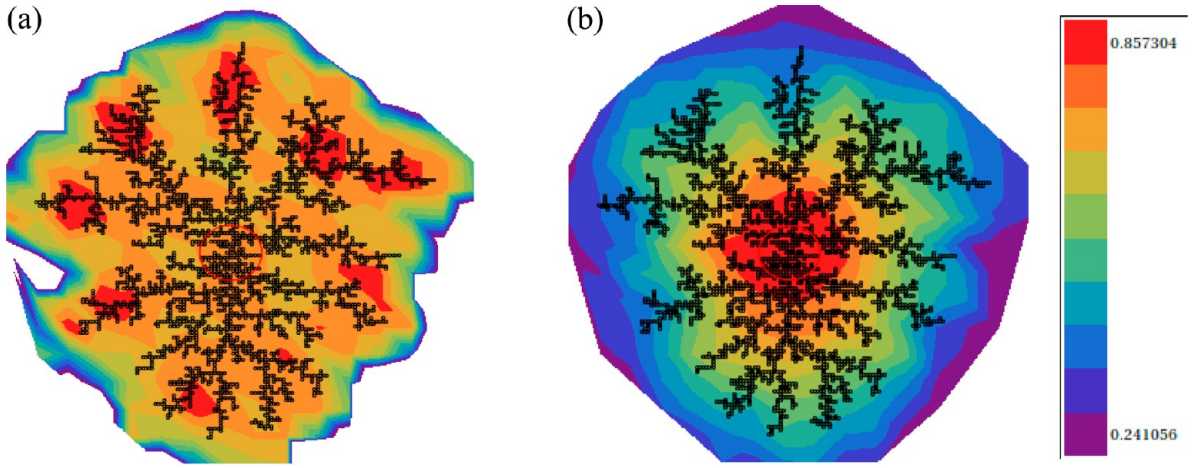

Figure 7. Calculated lifetime maps for generated DLA fractal clusters of monosize QDs, for two values of the Förster radius (expressed in units of the QD radius): (a) $R_F/R = 1$, (b) $R_F/R = 5$.

that the energy transfer processes do take place among nominally monosize CdSe and CdTe dots, in accordance with previous observations,[22,23] and can lead to important consequences predicted by our "minimal model" considering identical QDs assembled into DLA fractal clusters. By means of our model calculations based on master equations, we found that for a small Förster radius no significant energy transfer within the superstructure takes place, and the exciton transport is limited to some spots in the edges of the dendrite. However, for a sufficiently large R_F the excitons are clearly funneled into the (denser) core of the structure; i.e., the energy transfer is directed from the edges toward to the center. This effect is due to the reversibility of the Förster transfer processes between QDs of (approximately) equal size, leading to the anisotropy of the exciton fluxes in a structure with space-dependent density. The theoretical results are in line with the experimental findings comparing a system with a small Förster radius (CdSe) and a large Förster radius (CdTe) by mapping the fluorescence decay throughout the fractal dendrite shaped structures. In view of these experimental and theoretical results, self-assembled dendrite structures prepared from nominally monosize QDs are potentially interesting for light harvesting and spatially concentrated light emission or even for solid state cooling if interdot transfer processes are accompanied by an energy upconversion due to the participation of phonons.[47]

■ ASSOCIATED CONTENT

Supporting Information

A description of the autocorrelation function of dendrite images, spectral dependence of the PL decay kinetics, and additional data on FLIM and emission intensity maps. This material is available free of charge via the Internet at http://pubs.acs.org.

■ AUTHOR INFORMATION

Corresponding Author

*E-mail mouraisabel1@gmail.com; Tel 00351-253604060; Fax 00351-253604061 (I.M.).

Notes

The authors declare no competing financial interest.

■ ACKNOWLEDGMENTS

Financial support from the Portuguese Foundation for Science and Technology (FCT) and FEDER through Projects PTDC-FIS-113199-2009 and PEst-C/FIS/UI0607/2013 is gratefully acknowledged. All authors would like to thank Prof. Yury Rakovich.

■ ADDITIONAL NOTE

[a]For a monoexponential decay (for our model this corresponds to the case when the QD is isolated), PDF is just a δ-function, and its moments plotted as $\gamma^n\langle\tau^n\rangle$ are all equal to unity. For a uniform distribution, $\gamma^n\langle\tau^n\rangle \propto 1/n$.

■ REFERENCES

(1) Rogach, A. L., Ed.; *Semiconductor Nanocrystal Quantum Dots: Synthesis, Assembly, Spectroscopy and Applications*; Springer: New York, 2008.

(2) Klar, T. A.; Franzl, T.; Rogach, A. L.; Feldmann, J. Super-Efficient Exciton Funneling in Layer-by-Layer Semiconductor Nanocrystal Structures. *Adv. Mater.* **2005**, *17*, 769−773.

(3) Lin, X. M.; Jaeger, H. M.; Sorensen, C. M.; Klabund, K. J. Formation of Long-Range-Ordered Nanocrystal Superlattices on Silicon Nitride Substrates. *J. Phys. Chem. B* **2001**, *105*, 3353−3357.

(4) Murray, C. B.; Sun, S.; Gaschler, W.; Doyle, H.; Betley, T. A.; Kagan, C. R. Colloidal Synthesis of Nanocrystals and Nanocrystal Superlattices. *IBM J. Res. Dev.* **2001**, *45*, 47−56.

(5) Narayanan, S.; Wang, J.; Lin, X.-M. Dynamical Self-Assembly of Nanocrystal Superlattices during Colloidal Droplet Evaporation by in Situ Small Angle X-Ray Scattering. *Phys. Rev. Lett.* **2004**, Vol. *93*, 135503.

(6) Stein, H. N. Controlled Colloid Formation. *Curr. Opin. Colloid Interface Sci.* **1997**, *2*, 165−170.

(7) Volkov, Y.; Mitchell, S.; Gaponik, N.; Rakovich, Y. P.; Donegan, J. F.; Kelleher, D.; Rogach, A. L. In-Situ Observation of Nanowire Growth from Luminescent CdTe Nanocrystals in a Phosphate Buffer Solution. *ChemPhysChem* **2004**, *5*, 1600−1602.

(8) Sukhanova, A.; Baranov, A. V.; Klinov, D.; Oleinikov, V.; Berwick, K.; Cohen, J. H.; Pluot, M.; Nabiev, I. Self-Assembly of Charged Microclusters of CdSe/ZnS Core/Shell Nanodots and Nanorods into Hierarchically Ordered Colloidal Arrays. *Nanotechnology* **2006**, *17*, 4223−4228.

(9) Sukhanova, A.; Baranov, A. V.; Perova, T. S.; Cohen, J. H.; Nabiev, I. Controlled Self-Assembly of Nanocrystals into Polycrystalline Fluorescent Dendrites with Energy-Transfer Properties. *Angew. Chem., Int. Ed.* **2006**, *45*, 2048−2052.

(10) Sukhanova, A.; Volkov, Y.; Rogach, A. L.; Baranov, A. V.; Susha, A. S.; Klinov, D.; Oleinikov, V.; Cohen, J. H.; Nabiev, I. Lab-in-a-Drop: Controlled Self-Assembly of CdSe/ZnS Quantum Dots and Quantum Rods into Polycrystalline Nanostructures with Desired Optical Properties. *Nanotechnology* **2007**, *18*, 185602.
(11) Bigioni, T. P.; Lin, X.-M.; Nguyen, T. T.; Corwin, E. I.; Witten, T. A.; Jaeger, H. M. Kinetically-Driven Self-Assembly of Highly-Ordered Nanoparticle Monolayers. *Nat. Mater.* **2006**, *5*, 265−270.
(12) Rabani, E.; Reichman, D. R.; Geissler, P. L.; Brus, L. E. Drying-Mediated Self-assembly of Nanoparticles. *Nature* **2003**, *426*, 271−274.
(13) Gelbart, W. M.; Sear, R. P.; Heath, J. R.; Chaney, S. Array Formation in Nano-colloids: Theory and Experiment in 2D. *Faraday Discuss.* **1999**, *112*, 299−307.
(14) Förster, Th. Intermolecular Energy Migration and Fluorescence. *Ann. Phys.* **1948**, *437*, 55−75.
(15) Kagan, C. R.; Murray, C. B.; Nirmal, M.; Bawendi, M. G. Electronic Energy Transfer in CdSe Quantum Dot Solids. *Phys. Rev. Lett.* **1996**, *76*, 1517−1520.
(16) Komarala, V. K.; Bradley, A. L.; Rakovich, Y. P.; Byrne, S. J.; Guńko, Y. K.; Rogach, A. L. Enhanced Förster Resonance Energy Transfer between the CdTe Quantum Dots in Proximity to Gold Nanoparticles. *Proc. SPIE* **2007**, *6641*, 66410Y/1−66410Y/8.
(17) Franzl, T.; Shavel, A.; Rogach, A. L.; Gaponik, N.; Klar, T. A.; Eychmüller, A.; Feldmann, J. High Rate Unidirectional Energy Transfer in Directly Assembled CdTe Nanocrystal Bilayers. *Small* **2005**, *1*, 392−395.
(18) Guo, L.; Krauss, T. D.; Poitras, C. B.; Lipson, M.; Teng, X.; Yang, H. Energy Transfer Between Colloidal Semiconductor Nanocrystals in an Optical Microcavity. *Appl. Phys. Lett.* **2006**, *89*, 061104/1−061104/3.
(19) Clark, S. W.; Harbold, J. M.; Wise, F. W. Resonant Energy Transfer in PbS Quantum Dots. *J. Phys. Chem. C* **2007**, *111*, 7302−7305.
(20) Crooker, S. A.; Hollingsworth, J. A.; Tretiak, S.; Klimov, V. I. Spectrally Resolved Dynamics of Energy Transfer in Quantum-Dot Assemblies: Towards Engineered Energy Flows in Artificial Materials. *Phys. Rev. Lett.* **2002**, *89*, 186802.
(21) Lunz, M.; Bradley, A. L.; Chen, W-Yu.; Gerard, V. A.; Byrne, S. J.; Gun'ko, Y. K.; Lesnyak, V.; Gaponik, N. Influence of Quantum Dot Concentration on Förster Resonant Energy Transfer in Monodispersed Nanocrystal Quantum Dot Monolayers. *Phys. Rev. B* **2010**, *81*, 205316.
(22) Lunz, M.; Bradley, A. L.; Gerard, V. A.; Byrne, S. J.; Gun'ko, Y. K.; Lesnyak, V.; Gaponik, N. Concentration Dependence of Förster Resonant Energy Transfer Between Donor and Acceptor Nanocrystal Quantum Dot Layers: Effect of Donor-Donor Interactions. *Phys. Rev. B* **2011**, *83*, 115423.
(23) Shafiei, F.; Ziama, S. P.; Curtis, E. D.; Decca, R. S. Measurement of the Separation Dependence of Resonant Energy Transfer Between CdSe/ZnS Core/Shell Nanocrystallite Quantum Dots. *Phys. Rev. B* **2011**, *84*, 075301−075308.
(24) Shepherd, D. P.; Whitcomb, K. J.; Milligan, K. K.; Goodwin, P. M.; Gelfand, M. P.; Orden, A. V. Fluorescence Intermittency and Energy Transfer in Small Clusters of Semiconductor Quantum Dots. *J. Phys. Chem. C* **2010**, *114*, 14831−14837.
(25) Adrianov, V. E.; Maslov, V. G.; Baranov, A. V.; Fedorov, A. V.; Artemýev, M. V. Spectral Study of the Self-Organization of Quantum Dots During the Evaporation of Colloidal Solutions. *J. Opt. Technol.* **2011**, *78*, 699−705.
(26) Melnikau, D.; Savateeva, D.; Lesnyak, V.; Gaponik, N.; Fernández, Y. N.; Vasilevskiy, M. I.; Costa, M. F.; Mochalov, K. E.; Oleinikov, V.; Rakovich, Y. P. Resonance Energy Transfer in Self-Organized Organic/Inorganic Dendrite Structures. *Nanoscale* **2013**, *5*, 9317−9323.
(27) Santos, J. R.; Vasilevskiy, M. I.; Filonovich, S. A. Cascade Upconversion of Photoluminescence in Quantum Dot Ensembles. *Phys. Rev. B* **2008**, *78*, 245422.
(28) Dewey, T. G.; Datta, M. M. Determination of the Fractal Dimension of Membrane Protein Aggregates Using Fluorescence Energy Transfer. *Biophys. J.* **1989**, *56*, 415−420.
(29) Garcia, A. M. F.; Fernandes, M. S. F.; Coutinho, P. J. G. CdSe/TiO_2 Core-Shell Nanoparticles Produced in AOT Reverse Micelles: Applications in Pollutant Photodegradation Using Visible Light. *Nanoscale Res. Lett.* **2011**, *6*, 426−429.
(30) Byrne, S. J.; Corr, S. A.; Rakovich, T. Y.; Guńko, Y. K.; Rakovich, Y. P.; Donegan, J. F.; Mitchell, S.; Volkov, Y. Optimisation of the Synthesis and Modification of CdTe Quantum Dots for Enhanced Live Cell Imaging. *J. Mater. Chem.* **2006**, *16*, 2896−2902.
(31) Farinha, J. P. S.; Martinho, J. M. G. Resonance Energy Transfer in Polymer Nanodomains. *J. Phys. Chem. C* **2008**, *112*, 10591−10601.
(32) López, F.; Ojeda, P.; Arbeloa, I. Fluorescence Self-Quenching of the Molecular Forms of Rhodamine B in Aqueous and Ethanolic Solutions. *J. Lumin.* **1989**, *44*, 105−112.
(33) Mandelbrot, B. B. *The Fractal Geometry of Nature*; W.H. Freeman: New York, 1982.
(34) Jones, M.; Scholes, G. D. On the Use of Time-Resolved Photoluminescence as a Probe of Nanocrystal Photoexcitation Dynamics. *J. Mater. Chem.* **2010**, *20*, 3533−3538.
(35) Menezes, F.; Fedorov, A.; Baleizão, C.; Valeur, B.; Berberan-Santos, M. N. Methods for the Analysis of Complex Fluorescence Decays: Sum of Becquerel Functions Versus Sum of Exponentials. *Methods Appl. Fluoresc.* **2013**, *1*, 015002.
(36) Berberan-Santos, M. N.; Bodunov, E. N.; Valeur, B. Mathematical Functions for the Analysis of Luminescence Decays with Underlying Distributions I. Kohlrausch Decay Function (Stretched Exponential). *Chem. Phys.* **2005**, *315*, 171−182; II. Becquerel (Compressed Hyperbola) and Related Decay Functions. *Chem. Phys.* **2005**, *317*, 57−62.
(37) Rolinski, O. J.; Birch, D. J. S. Determination of Acceptor Distribution from Fluorescence Resonance Energy Transfer: Theory and Simulation. *J. Chem. Phys.* **2000**, *112*, 8923−8933.
(38) Wolber, P. K.; Hudson, B. S. An Analytic Solution to the Förster Energy Transfer Problem in Two Dimensions. *Biophys. J.* **1979**, *28*, 197−210.
(39) Pines, D.; Huppert, D. Electronic Energy Transport and Trapping on Fractals. *J. Chem. Phys.* **1989**, *91*, 7291.
(40) Even, U.; Rademann, K.; Jortner, J.; Manor, N.; Reisfeld, R. Electronic Energy Transfer on Fractals. *Phys. Rev. Lett.* **1984**, *52*, 2164−2167.
(41) Scholes, G. D.; Andrews, D. L. Resonance Energy Transfer and Quantum Dots. *Phys. Rev. B* **2005**, *72*, 125331−125338.
(42) Lyo, S. K. Spectral and Spatial Transfer and Diffusion of Excitons in Multiple Quantum Dot Structures. *Phys. Rev. B* **2009**, *79*, 125328.
(43) Witten, T. A.; Sander, L. M. Diffusion-Limited Aggregation: A Kinetic Critical Phenomenon. *Phys. Rev. Lett.* **1981**, *47*, 1400−1403.
(44) Yu, W. W.; Qu, L.; Guo, W.; Peng, X. Experimental Determination of the Extinction Coefficient of CdTe, CdSe and CdS Nanocrystals. *Chem. Mater.* **2003**, *15*, 2854−2860.
(45) Fernández, Y. N.; Vasilevskiy, M. I; Larramendi, E. M.; Trallero-Giner, C. *Fingerprints in the Optical and Transport Properties of Quantum Dots*; ISBN 978-953-51-0648-7, InTech - Open Access Publisher, 2012.
(46) Förster, Th. Experimentelle und Theoretische Untersuchubg des Zwischenmolekularen Ubergangs Von Elektronenanregungsenergie. *Z. Naturforsch., Sect. A* **1949**, *4*, 321−327.
(47) Rakovich, Y. P.; Donegan, J. F.; Vasilevskiy, M. I.; Rogach, A. L. Anti-Stokes Cooling in Semiconductor Nanocrystal Quantum Dots: A Feasibility Study. *Phys. Status Solidi A* **2009**, *206*, 2497−2509.